Rajamaki, Robin; Koivunen, Visa

Symmetric sparse linear array for active imaging

Published in:
2018 IEEE 10th Sensor Array and Multichannel Signal Processing Workshop, SAM 2018

DOI:
10.1109/SAM.2018.8448767

Published: 27/08/2018

Document Version
Peer-reviewed accepted author manuscript, also known as Final accepted manuscript or Post-print

Please cite the original version:
Rajamaki, R., & Koivunen, V. (2018). Symmetric sparse linear array for active imaging. In *2018 IEEE 10th Sensor Array and Multichannel Signal Processing Workshop, SAM 2018* (Vol. 2018-July, pp. 46-50). Article 8448767 (Proceedings of the IEEE Sensor Array and Multichannel Signal Processing Workshop). IEEE. https://doi.org/10.1109/SAM.2018.8448767

Symmetric Sparse Linear Array for Active Imaging

Robin Rajamäki and Visa Koivunen
Department of Signal Processing and Acoustics
School of Electrical Engineering, Aalto University, 02150 Espoo, Finland
Email: robin.rajamaki@aalto.fi, visa.koivunen@aalto.fi

***Abstract*—*Sparse sensor arrays* can achieve significantly more degrees of freedom than the number of elements by leveraging the *co-array*, a virtual structure that arises from the far field narrowband signal model. Although several sparse array configurations have been developed for passive sensing tasks, less attention has been paid to arrays suitable for active sensing. This paper presents a novel active sparse linear array, called the *Interleaved Wichmann Array* (IWA). The IWA only has a few closely spaced elements, which may make it more robust to mutual coupling effects. Closed-form expressions are provided for the key properties of the IWA. The parameters maximizing the array aperture for a given even number of elements are also found. The near field wideband performance of the array is demonstrated numerically in a coherent imaging scenario.**

I. Introduction

Sparse sensor arrays offer a cost effective alternative to conventional filled arrays with uniformly spaced sensors. By utilizing the *degrees of freedom* (DOF) provided by the co-array [1], sparse arrays can e.g. match the *point spread function* (PSF) in imaging applications, or resolve the same number of sources in direction finding tasks as a filled array of equivalent aperture [2], [3]. Since only $\mathcal{O}(N)$ physical elements are necessary to represent $\mathcal{O}(N^2)$ co-array elements, sparse arrays with significantly fewer sensors and RF front ends may achieve the same number of DOFs as filled arrays. Sparse arrays also have fewer closely spaced elements, which can improve performance in presence of mutual coupling [4], [5].

Sparse array design is often concerned with finding array configurations with a desired co-array, using as few physical elements as possible. In the case of linear arrays, the target co-array is usually the *Uniform Linear Array* (ULA), which maximizes the number of DOF in the co-array of a given aperture, when the physical elements are constrained to a uniform grid. A uniform co-array allows for efficient array processing algorithms to be employed, and avoids grating lobes in the beampattern when the virtual elements are spaced at most half a wavelength apart. The array minimizing the number of elements subject to a ULA co-array is called the *Minimum-Redundancy Array* (MRA) [6], [7]. The MRA is however impractical to find for large array apertures, and lacks a closed-form expression for its sensor positions. This has encouraged research into finding analytically tractable, but possibly sub-optimal array configurations, such as the Wichmann [8], Nested [9] and Co-prime arrays [10]. Many of these configurations have a *difference co-array* with the ULA property, which is desirable in passive sensing applications like DOA estimation [9]. However, the *sum co-array* of these arrays often contains holes, which may degrade performance in active sensing tasks, such as coherent imaging [2]. The largest known MRA with a ULA sum co-array has $N = 48$ elements [11], [12]. Beyond this, other active sparse array configurations have to be considered. The *Reduced-Redundancy Array* (RRA) [7] is one solution that combines several smaller MRAs into a larger sparse array. Unfortunately, the number of elements N in the RRA scales linearly with aperture L, whereas $N \propto \sqrt{L}$ would be preferable. A modification of the Nested Array [9], called the *Concatenated Nested Array* (CNA), was recently proposed to address this problem [13]. However, the CNA still has many closely spaced elements, which may degrade performance when mutual coupling is considered.

This paper introduces a novel sparse active linear array configuration with fewer closely spaced elements than the CNA. The proposed *Interleaved Wichmann Array* (IWA) consists of the union of a *Wichmann Array* (WA) [8] and its mirror image. The facts that the difference co-array of the WA is a ULA and the IWA is symmetric, guarantee that the sum and difference co-arrays of the IWA are ULAs [14]. Closed-form parametric expressions are derived for the element positions and key properties of the IWA. Furthermore, the parameters maximizing the array aperture for a given even number of elements are found. Finally, the near field wideband imaging performance of the array is demonstrated numerically.

The paper is organized as follows: Section II reviews the active imaging signal model, and the sum co-array. Section III presents the IWA, its properties, and a derivation of its optimal parameters. In section IV, the IWA is compared the ULA in a coherent imaging simulation. Section V concludes the paper.

II. Signal model

A. Active coherent imaging

Consider a linear array with N omnidirectional transceivers at $\mathcal{D} = \{\tilde{d} \cdot i_n \mid i_n \in \mathbb{Z}\}_{n=1}^{N}$, where $\mathbb{Z}$ is the set of integers, and $\tilde{d}$ is the unit inter-element spacing (typically half a wavelength). The array is used to image a collection of K coherent, possibly near field, point reflectors. The scenario is illustrated in Fig. 1 for a single transmitter (Tx), receiver (Rx), and target. A pulse $p(t) = s(t)e^{j\omega_c t}$, with carrier frequency ω_c and amplitude $s(t) \in \mathbb{C}$, where $\mathbb{C}$ is the set of complex numbers, is transmitted from the m^{th} transmitter, and scattered by the k^{th} target with reflectivity $\gamma_k \in \mathbb{C}$. The signal is then received at the n^{th} receiver after delay $\tau_{mnk} = (l_{mk} + l_{nk})/c$, where c denotes the wave propagation speed. In the absence of clutter and receiver noise, the received signal is:

$$x_{mn}(t) = \sum_{k=1}^{K} \gamma_k s(t - \tau_{mnk}) e^{j\omega_c (t - \tau_{mnk})}. \quad (1)$$

Target reflectivity is assumed to be frequency independent. Higher order reflections, propagation losses and mutual cou-

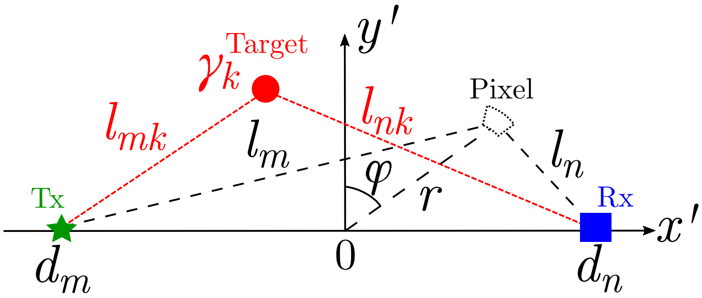

Fig. 1. Active imaging in the plane. Element positions are given by d_i, distances by l_i and target reflectivities by γ_k.

pling are also ignored. The distance between the n^{th} element of the array located at $d_n \in \mathcal{D}$, and a point with polar coordinates (r, φ) is $l_n = \sqrt{r^2 + d_n^2 - 2rd_n \sin(\varphi)}$. The array is focused by delaying the received signals in (1) by $\tau_{mn}(\varphi, r) = (l_m(r, \varphi) + l_n(r, \varphi))/c$. The delayed signals are then weighted by transmit and receive weights $w_{\mathrm{t},m}, w_{\mathrm{r},n} \in \mathbb{C}$ and summed, yielding the beamformed signal:

$$y(t, r, \varphi) = \sum_{m=1}^{N} \sum_{n=1}^{N} w_{\mathrm{t},m} w_{\mathrm{r},n} x_{mn}(t + \tau_{mn}(r, \varphi)). \quad (2)$$

Matched filtering of (2) with the transmitted pulse p produces an estimate of the reflectivity at (r, φ). The output of the matched filter sampled at $\tau = 0$ is $\hat{\gamma}(r, \varphi) = \int_{-\infty}^{\infty} p^*(t - \tau) y(t, r, \varphi) dt \mid_{\tau=0}$. This evaluates to

$$\hat{\gamma}(r, \varphi) = \sum_{m=1}^{N} \sum_{n=1}^{N} w_{\mathrm{t},m} w_{\mathrm{r},n} \sum_{k=1}^{K} \gamma_k e^{j\omega_c \Delta\tau_{mnk}} R_{ss}(\Delta\tau_{mnk}), \quad (3)$$

where $R_{ss}(\tau)$ is the autocorrelation function of the baseband signal $s(t)$. Delay $\Delta\tau_{mnk} = \tau_{mn}(r, \varphi) - \tau_{mnk}$ denotes the difference between the focusing delay of the current pixel and the round-trip delay to the k^{th} target.

B. Sum co-array

The co-array is a virtual array structure arising from (3). Particularly, the sum co-array emerges when the target range $r_k \to \infty\ \forall k$. In this far field case, the delay difference simplifies to $\Delta\tau_{mnk} = (d_m + d_n)(u_k - u)/c$, where $u = \sin(\varphi)$ [15]. Thus (3) becomes a function of the sum co-array [2]:

$$\mathcal{C}_\Sigma = \{d_\Sigma = d_n + d_m \mid d_n, d_m \in \mathcal{D}\}. \quad (4)$$

Several element pairs may contribute to the same co-array element. Consequently, the *multiplicity* or *natural weighting* of the sum co-array may be defined as $\upsilon_\Sigma(d_\Sigma) = \sum_{d_m, d_n \in \mathcal{D}} \mathbb{1}(d_\Sigma = d_m + d_n)$, where $\mathbb{1}(\cdot)$ is the indicator function. For convenience, $\mathcal{D}$ is often normalized by the unit spacing $\tilde{d}$ and shifted such that a set of non-negative integers $\mathcal{D} \subseteq \{0, 1, \ldots, L\}$ is obtained. It follows that $\mathcal{C}_\Sigma \subseteq \{0, 1, \ldots, 2L\}$. The sum co-array is said to be *contiguous* when it has no holes, i.e. $\mathcal{C}_\Sigma = \{0, 1, \ldots, 2L\}$. Two arrays are *co-array equivalent* when they have the same co-array support.

1) Wideband effects: The frequency dependence of the co-array is revealed through the Fourier transform relationship between the autocorrelation function R_{ss} and *power spectral density* (Wiener-Khinchin theorem): $R_{ss}(\tau) = \int_{-\infty}^{\infty} s(t)s^*(t + \tau)dt = \int_{-\infty}^{\infty} |S(f)|^2 e^{j2\pi f \tau} df$. Here, $S(f)$ is the Fourier transform of $s(t)$. Substituting the expression into (3) yields $\hat{\gamma}(r, u) \propto e^{j2\pi(f_c + f)\Delta\tau_{mnk}}$. The factor $(f_c + f)\Delta\tau_{mnk}$ determines the *wideband co-array*, which now clearly also depends on the temporal frequency. In the far field $(f_c + f)\Delta\tau_{mnk} = \alpha(d_m + d_n)(u_k - u)/\lambda_c$, where $\alpha = (f_c + f)/f_c$ and λ_c is the carrier wavelength. The far field wideband co-array is thus the union of scaled copies of the narrowband co-array in (4) [16]:

$$\mathcal{C}_{\Sigma,\mathrm{fw}} = \bigcup\nolimits_f \alpha\mathcal{C}_\Sigma. \quad (5)$$

In other words, the co-array is contracted or expanded by a scale factor α for each frequency component in the spectrum of the transmitted pulse.

2) Near field effects: The impact of near field targets on the co-array can be analyzed by retaining the two leading-order terms of the Taylor expansion of the focusing delay [15]. This yields $\tau_{mn} \approx (2r - (d_m + d_n)u + (d_m^2 + d_n^2)(1 - u^2)/(2r))/c$. The delay difference $\Delta\tau_{mnk}$ for a target in range focus, i.e. $r = r_k$, then evaluates to [15]: $\Delta\tau_{mnk} \approx ((d_m + d_n) + (d_m^2 + d_n^2)(u_k + u)/(2r))(u_k - u)/c$. Consequently, there is a coupling between target range, direction and array geometry in the near field. In the narrowband case, this is captured by the *spatially varying co-array* [17]:

$$\mathcal{C}_{\Sigma,\mathrm{nn}} \approx \{d_m + d_n + \tfrac{1}{2r}(d_m^2 + d_n^2)(u_k + u) \mid d_n, d_m \in \mathcal{D}\}. \quad (6)$$

The more general near field wideband co-array is obtained by combining (5) and (6), yielding $\mathcal{C}_{\Sigma,\mathrm{nw}} \approx \bigcup_f \alpha\mathcal{C}_{\Sigma,\mathrm{nn}}$.

C. Image addition

Image addition is a co-array processing technique that enables co-array equivalent arrays to achieve the same set of PSFs [2], [18]. The idea is that a desired *co-array weighting* υ is synthesized as the sum of component co-array weightings υ_q. Weighting υ replaces the natural weighting υ_Σ, which might produce an unsatisfactory PSF with high side lobes. The components υ_q are given by the convolution between different sets of transmit-receive weight pairs, i.e. $\upsilon[i] = \sum_{q=1}^{Q} \upsilon_q[i] = \sum_{q=1}^{Q} (\tilde{w}_{\mathrm{t},q} * \tilde{w}_{\mathrm{r},q})[i]$. The number of component images Q determines the accuracy of the synthesis, since sequences $\tilde{w}_{\mathrm{t},q}$ and $\tilde{w}_{\mathrm{r},q}$ are sparse when the array is sparse. A perfect synthesis is guaranteed when Q equals the number of sensors N [18]. Fewer components may also be sufficient, depending on υ and the desired accuracy of the synthesis. The number of components affects the frame rate of the imaging system, and should therefore be kept low [19].

III. Interleaved Wichmann Array

This section introduces the *Interleaved Wichmann Array* (IWA) and establishes some of its key properties, such as aperture, number of elements and number of unit spacings. Sensor positions of the IWA are given in closed-form, and the array parameters that maximize the aperture for a given even number of elements are derived.

The *Wichmann Array* (WA) is based on a pattern of restricted difference bases first reported in [8]. Restricted difference bases [20] are essentially the number theoretical equivalent of Minimum-Redundancy Arrays [6] in passive array processing. The Wichmann pattern was later rediscovered

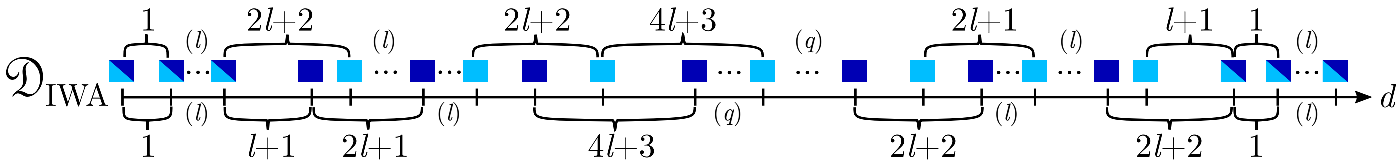

Fig. 2. The Interleaved Wichmann Array (IWA) is the union of a Wichmann Array (WA) [8] (dark elements) and its mirror image (light elements). Parameters $l, q \in \mathbb{N}$ control the distance between consecutive elements in the WA (braces), and the number of times these distances are repeated (parenthesis).

and adapted to sparse sensor arrays in [21], [22]. The WA has three desirable properties: low redundancy, few unit inter-element spacings, and a contiguous difference co-array [23]. Unfortunately, the WA is less suitable for active sensing, since its sum co-array contains holes. However, the IWA defined by the union of a WA with its mirror image, has a contiguous sum co-array. This follows from the symmetry of the IWA, and the contiguous difference co-array property of the WA, see Lemma 1 in [14]. Fig. 2 illustrates the structure of the IWA. The formal definition of the IWA is:

Definition 1 (Interleaved Wichmann array (IWA)): The element positions of the IWA are given by $\mathcal{D}_{\mathrm{IWA}} = \mathcal{D}_{\mathrm{WA}} \cup \mathcal{D}_{\mathrm{WA}^-}$, where $\mathcal{D}_{\mathrm{WA}} = 0 \cup \{\sum_{i=1}^{n} \Delta d_{\mathrm{WA}}[i]\}_{n=1}^{4l+q+2}$, $\mathcal{D}_{\mathrm{WA}^-} = 4l(l+q+2)+3(q+1)-\mathcal{D}_{\mathrm{WA}}$ and $\Delta d_{\mathrm{WA}} = 1^{\times(l)}, l+1, (2l+1)^{\times(l)}, (4l+3)^{\times(q)}, (2l+2)^{\times(l+1)}, 1^{\times(l)}$. Parameters l and q are non-negative integers, i.e $l, q \in \mathbb{N}$.

The sequence Δd_{WA} denotes the spacings between consecutive elements in the WA, and the notation $a^{\times(b)}$ is shorthand for "a repeated b times". Consequently Δd_{WA} has $4l+q+2$ entries, with a cumulative sum of $4l(l+q+2)+3(q+1)$, which equals the aperture of both the WA and IWA.

A. Properties of IWA

It can be seen from Fig. 2 that only $2(l+1)$ elements of the two Wichmann sub-arrays $\mathcal{D}_{\mathrm{WA}}$ and $\mathcal{D}_{\mathrm{WA}^-}$ overlap. By definition, the number of elements N in the IWA is even and ≥ 4, or more precisely:

$$N = 2(3l+q+2). \tag{7}$$

The array aperture remains the same as for the WA, that is:

$$L = 4l(l+q+2)+3(q+1). \tag{8}$$

Furthermore, the number of unit spacings in the IWA is:

$$\upsilon_{\Delta}(1) = \begin{cases} q+3, & \text{when } l = 0 \\ 2l+2, & \text{otherwise.} \end{cases} \tag{9}$$

This is slightly higher than for the WA which has $\upsilon_{\Delta}(1) = 2l$ when $l \geq 1$, and $\upsilon_{\Delta}(1) = 1$ when $l = 0$. The proofs of (7) and (9) are provided in [24] due to lack of space here.

B. Optimization problem

Maximizing the DOF provided by the IWA is equivalent to finding parameters $l, q \in \mathbb{N}$ that maximize the aperture $L \in \mathbb{N}$ in (8) for a given even number of elements $N \geq 4$. This requires solving the following constrained optimization problem:

$$\begin{aligned} &\underset{l,q\in\mathbb{N}}{\text{maximize}} \quad 4l(l+q+2)+3(q+1) \\ &\text{subject to} \quad q = N/2-3l-2. \end{aligned} \tag{P1}$$

Note that the objective function of (P1) remains the same in the case of the WA, but the constraint is replaced by $q = N-3-4l$ [23]. Therefore, the optimal IWA does not necessarily consist of an optimal WA. (P1) is nevertheless a non-convex integer program, which appears challenging to solve. However, the problem admits a closed-form solution, as is shown next.

C. Relaxed solution

Solving (7) for q and substituting the result into (8) yields the new objective function:

$$L = -8l^2 + (2N-9)l + \tfrac{3}{2}N - 3. \tag{10}$$

Maximizing (10) subject to the relaxed constraint that $l, q \in \mathbb{R}_+$, where $\mathbb{R}_+$ is the set of non-negative real numbers, results in a concave unconstrained optimization problem with the solution $\tilde{l}^\star = (2N-9)/16$. Substitution into (7) yields $\tilde{q}^\star = (2N-5)/16$. It follows that $\tilde{l}^\star \notin \mathbb{N}$ when N is even. Even if $\tilde{l}^\star \in \mathbb{N}$, then clearly $\tilde{q}^\star = \tilde{l}^\star + 1/4 \notin \mathbb{N}$. Consequently, $\tilde{l}^\star$ and $\tilde{q}^\star$ must be projected to the set of integers in order to obtain a feasible solution to (P1), as is done next.

D. General solution

Since (10) is concave when $l \in \mathbb{R}_+$, the optimal integer-valued parameter pair solving (P1) is

$$l^\star = \lfloor (2N-9)/16 \rceil \tag{11}$$
$$q^\star = N/2 - 3l^\star - 2, \tag{12}$$

where $\lfloor \cdot \rceil$ denotes rounding to the nearest integer. Note that $q^\star$ is always a non-negative integer. The integer property follows directly from the fact that N is even. The non-negativity is less obvious, but easily verifiable from (11) and (12). Due to the rounding operation in (11), the optimal l becomes

$$l^\star = (N/4 - \alpha)/2, \tag{13}$$

where α depends on the value of N (proof in [24]):

$$\alpha = \begin{cases} 1, & \text{when } N = 4+8m \\ 3/2, & \text{when } N = 6+8m \\ 2, & \text{when } N = 8+8m \\ 1/2, & \text{when } N = 10+8m, \end{cases} \tag{14}$$

and $m \in \mathbb{N}$. Substituting (13) into (10) yields the optimal aperture of the array, $L^\star = (N^2+3N-\beta)/8$, where $\beta = \{4, 6, 16, 10\}$ depends on the value of α in (14). A lower bound on number of elements is obtained by setting $\beta = 4$ and solving for N, yielding $N^\star \geq (\sqrt{32L+25}-3)/2 = \mathcal{O}(\sqrt{8L})$. For comparison, the CNA also achieves $N = \mathcal{O}(\sqrt{8L})$ [13]. Similarly, substituting (13) into (9) yields the number of unit spacings: $\upsilon_{\Delta}^\star(1) = N/2+1$, when $N \leq 8$, and $N/4+\zeta$ otherwise. Again, ζ depends on N as α and β, and assumes values $\zeta = \{1, 1/2, 0, 3/2\}$. Note that this is only half of the number of unit spacings in the CNA with $v_\Delta(1) \approx N/2$ [13].

IV. Coherent imaging example

Next, the performance of the IWA is demonstrated in a coherent imaging application. Both far and near field targets, as well as narrow and wideband signals are considered. "Near field" is understood as the Fraunhofer diffraction limit $r_\mathrm{f} = L^2/\lambda_\mathrm{c}$ [25], where L is the physical aperture of the array. The aperture is set to $L = 22 \cdot \lambda_\mathrm{c}/2$, and thus the Fraunhofer limit evaluates to $r_\mathrm{f} = 11L$. Fig. 3 shows the IWA with $N = 12$ elements, and the ULA of equivalent aperture with $N = 23$ elements. "Wideband" refers to a square pulse of length $T_p = N_\mathrm{cyc}\lambda_\mathrm{c}/c$, where N_cyc is the number of cycles of the carrier. The relative 3 dB bandwidth of such a signal is $B_\mathrm{rel} = B/f_\mathrm{c} \approx 0.88/N_\mathrm{cyc}$ [25]. The number of cycles is set to $N_\mathrm{cyc} = 10$, yielding $B_\mathrm{rel} \approx 0.088$. This could correspond to a 3 GHz microwave carrier with 264 MHz bandwidth, or a 1.5 MHz ultrasound carrier with 132 kHz bandwidth.

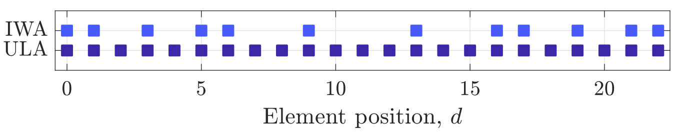

Fig. 3. Array configurations with aperture $L = 22 \cdot \lambda_\mathrm{c}/2$. The IWA has $N = 12$ elements compared to the ULA with $N = 23$ elements.

A triangular co-array weighting is selected. This window is achieved naturally by the ULA with unit gain transmit and receive weights. Fig. 4 shows the PSF obtained by the IWA using image addition. Side-lobes are over -20 dB for a single component image, whereas the desired PSF is achieved with $Q = 8$ component images.

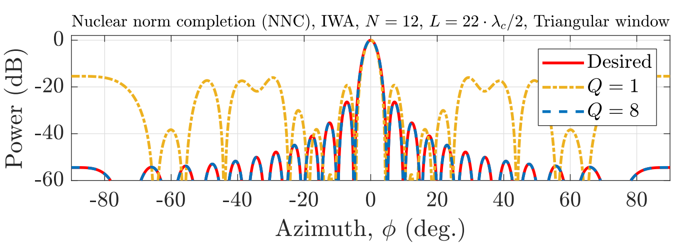

Fig. 4. Point spread function of IWA. Image addition with a single component ($Q = 1$) does not suppress the grating lobes of the sparse array. The desired PSF is achieved by increasing the number of components to $Q = 8$.

Fig. 5 shows the reflectivity estimate (3) of a single target with reflectivity $\gamma = 1$ in range focus of the array. Using image addition ($Q = 8$), the IWA is able to perfectly match the target PSF in the far field narrowband case shown in Fig. 5(a). In Fig. 5(b), the beampattern no longer has deep nulls due to the wideband co-array (5). However, the main lobe width and side lobe levels remain unaltered. In the near field, Fig. 5(c) and 5(d), the effects of the spatially varying co-array (6) become dominant. Image addition is unable to fully compensate for the grating lobes, although the performance is significantly better than with a single component image (Fig. 4).

Next, three near field targets are imaged with both the ULA and IWA. The target parameters are $r = \{109, 121, 133\}\lambda_\mathrm{c}$, $\varphi = \{-\pi/4, 0, \pi/4\}$ and $\gamma = \{1, 1, 1\}$. The SNR of a single receiving sensor in additive white Gaussian noise is 30 dB. Fig. 6 shows results after image addition with a single component image for the ULA and eight components for the IWA. The IWA shows close similarity with the ULA close to the targets, whereas side lobes appear further away, as expected based on Fig. 5(d). Since the IWA has fewer elements than the ULA, it also has a lower array gain. The SNR loss of the IWA compared to the ULA is $\approx -30\log(12/23) \approx 8.5$ dB [14].

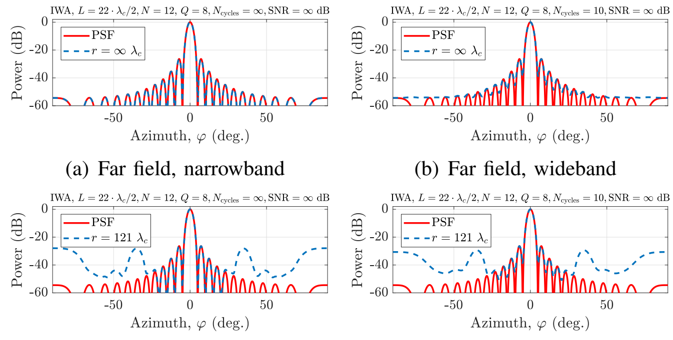

(a) Far field, narrowband (b) Far field, wideband

(c) Near field, narrowband (d) Near field, wideband

Fig. 5. IWA response to single target at boresight. In (a), the desired PSF is perfectly matched under far field narrowband conditions. In (b), the wideband signal smears out the nulls, but do not degrade side lobe levels or main lobe width. In (c) and (d), near field effects dominate and produce grating lobes.

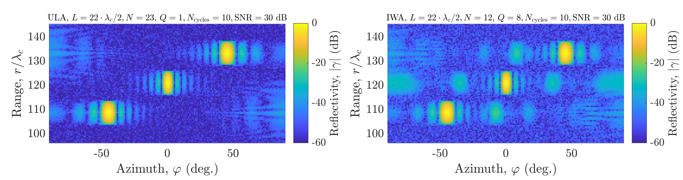

(a) ULA (b) IWA

Fig. 6. Image of three targets located at a distance of $10-12$ array apertures from the array baseline. The (a) ULA and (b) IWA have identical responses for small angular deviations around the target, whereas image addition is unable to suppress grating lobes when the angle becomes too large. The IWA has 50% fewer elements than the ULA, and as a consequence, lower image SNR.

V. Conclusion

This paper introduced the Interleaved Wichmann Array (IWA), a sparse linear array for active sensing. The optimal sensor placements of the array were derived, and relevant properties were established. The IWA halves the number of unit spacings of the recently proposed Concatenated Nested Array, whilst retaining approximately the same number of elements. Consequently, the IWA may be less sensitive to mutual coupling. Additionally, the IWA is both difference and sum co-array equivalent with the uniform linear array (ULA) of equal aperture. This property enables the IWA to match the point spread function of the ULA in the far field, while only suffering an inevitable SNR loss due to having fewer elements. Grating lobes resulting from the non-uniform element spacing limit the performance of the array in the near field. Further research into co-array processing is required to address this issue. In future work, it would also be interesting to investigate symmetric sparse arrays based on other geometries than the Wichmann array. Furthermore, exploring non-trivial extensions of the IWA with an odd number of elements could be relevant.

References

[1] R. A. Haubrich, "Array design," *Bulletin of the Seismological Society of America*, vol. 58, no. 3, pp. 977–991, 1968.

[2] R. T. Hoctor and S. A. Kassam, "The unifying role of the coarray in aperture synthesis for coherent and incoherent imaging," *Proceedings of the IEEE*, vol. 78, no. 4, pp. 735–752, Apr 1990.

[3] ——, "High resolution coherent source location using transmit/receive arrays," *IEEE Transactions on Image Processing*, vol. 1, no. 1, pp. 88–100, Jan 1992.

[4] E. BouDaher, F. Ahmad, M. G. Amin, and A. Hoorfar, "Mutual coupling effect and compensation in non-uniform arrays for direction-of-arrival estimation," *Digital Signal Processing*, vol. 61, pp. 3–14, 2017.

[5] C. L. Liu and P. P. Vaidyanathan, "Super nested arrays: Linear sparse arrays with reduced mutual coupling - part I: Fundamentals," *IEEE Transactions on Signal Processing*, vol. 64, no. 15, pp. 3997–4012, Aug 2016.

[6] A. Moffet, "Minimum-redundancy linear arrays," *IEEE Transactions on Antennas and Propagation*, vol. 16, no. 2, pp. 172–175, Mar 1968.

[7] R. T. Hoctor and S. A. Kassam, "Array redundancy for active line arrays," *IEEE Transactions on Image Processing*, vol. 5, no. 7, pp. 1179–1183, Jul 1996.

[8] B. Wichmann, "A note on restricted difference bases," *Journal of the London Mathematical Society*, vol. s1-38, no. 1, pp. 465–466, 1963.

[9] P. Pal and P. P. Vaidyanathan, "Nested arrays: A novel approach to array processing with enhanced degrees of freedom," *IEEE Transactions on Signal Processing*, vol. 58, no. 8, pp. 4167–4181, Aug 2010.

[10] P. P. Vaidyanathan and P. Pal, "Sparse sensing with co-prime samplers and arrays," *IEEE Transactions on Signal Processing*, vol. 59, no. 2, pp. 573–586, Feb 2011.

[11] J. Kohonen, "A meet-in-the-middle algorithm for finding extremal restricted additive 2-bases," *Journal of Integer Sequences*, vol. 17, no. 6, 2014.

[12] ——, "Early pruning in the restricted postage stamp problem," *arXiv preprint arXiv:1503.03416*, 2015.

[13] R. Rajamäki and V. Koivunen, "Sparse linear nested array for active sensing," in *25th European Signal Processing Conference (EUSIPCO 2017)*, Kos, Greece, August 2017.

[14] R. Rajamäki and V. Koivunen, "Sparse rectangular array with reduced mutual coupling for active sensing," *arXiv preprint arXiv:1803.02219*, 2018.

[15] R. J. Kozick and S. A. Kassam, "Synthetic aperture pulse-echo imaging with rectangular boundary arrays," *IEEE Transactions on Image Processing*, vol. 2, no. 1, pp. 68–79, Jan 1993.

[16] F. Ahmad and S. A. Kassam, "Coarray analysis of the wide-band point spread function for active array imaging," *Signal Processing*, vol. 81, no. 1, pp. 99–115, 2001.

[17] L. He and S. Kassam, "Near-range point spread function coarray analysis for array imaging," *IEEE Transactions on Aerospace and Electronic Systems*, vol. 51, no. 1, pp. 397–404, January 2015.

[18] R. J. Kozick and S. A. Kassam, "Linear imaging with sensor arrays on convex polygonal boundaries," *IEEE Transactions on Systems, Man, and Cybernetics*, vol. 21, no. 5, pp. 1155–1166, Sep 1991.

[19] R. Rajamäki and V. Koivunen, "Sparse array imaging using low-rank matrix recovery," in *Seventh IEEE International Workshop on Computational Advances in Multi-Sensor Adaptive Processing (CAMSAP 2017)*, Curaçao, Dutch Antilles, December 2017.

[20] J. Leech, "On the representation of $1, 2, \dots, n$ by differences," *Journal of the London Mathematical Society*, vol. s1-31, no. 2, pp. 160–169, 1956.

[21] D. Pearson, S. U. Pillai, and Y. Lee, "An algorithm for near-optimal placement of sensor elements," *IEEE Transactions on Information Theory*, vol. 36, no. 6, pp. 1280–1284, Nov 1990.

[22] D. A. Linebarger, I. H. Sudborough, and I. G. Tollis, "Difference bases and sparse sensor arrays," *IEEE Transactions on Information Theory*, vol. 39, no. 2, pp. 716–721, Mar 1993.

[23] R. Rajamäki and V. Koivunen, "Comparison of sparse sensor array configurations with constrained aperture for passive sensing," in *IEEE Radar Conference (RadarConf 2017)*, May 2017, pp. 0797–0802.

[24] ——, "Sparse linear arrays for active sensing," *Manuscript in preparation*, 2018.

[25] B. Steinberg, *Principles of aperture and array system design: Including random and adaptive arrays*. New York, Wiley-Interscience, 1976.